Journal of
Materials Chemistry A

Materials for energy and sustainability

Accepted Manuscript

This article can be cited before page numbers have been issued, to do this please use: Y. Gu, A. Wu, L. Wang, D. Wang, Y. Xie, H. Yan, P. Yu, C. Tian, F. Sun and H. Fu, *J. Mater. Chem. A*, 2020, DOI: 10.1039/C9TA13615K.

ROYAL SOCIETY OF CHEMISTRY

rsc.li/materials-a

View Article Online
DOI: 10.1039/C9TA13615K

Journal Name

ARTICLE

A "competitive occupancy" strategy toward Co-N_4 single-atom catalysts embedded in 2D TiN/rGO sheets for high-efficient and stable aromatic nitroreduction

Received 00th January 20xx,
Accepted 00th January 20xx

DOI: 10.1039/x0xx00000x

www.rsc.org/

Ying Gu,[a] Aiping Wu,[b] Lei Wang,[b] Dongxu Wang,[b] Haijing Yan,[b] Peng Yu,[b] Ying Xie,[b] Chungui Tian,*[b] Fanfei Sun[c] and Honggang Fu*[ab]

The single-atom catalysts (SACs) have been promising in catalytic fields, but the controllable synthesis of SACs with high stability remain challenging. Here, we show a robust strategy toward the highly-efficient and stable SACs based on "competitive occupancy" of two metal (M) species on graphite oxide (GO). The abundant M_1 (Ti) species predominantly occupy more groups of GO, thus leaving a tiny of groups at the gaps of M_1 species to combine with M_2 (Co^{2+} etc.) species, and consequently, guaranteeing the formation of Co-N_4 SACs embedded in 2D TiN/rGO sheets during the nitridation. Also, the TiN can act as a "spacer" to prevent Co-N_4 from aggregation, thus improving the stability of the catalyst. The Co-N_4/TiN-rGO exhibits outstanding catalytic performance for fast conversion of high-concentrated aromatic nitro compounds (0.3~2 mM) into amino compounds and excellent re-cycled ability, being at the forefront of reported catalysts. In contrast, the TiN/rGO has no obvious activity, and Co_4N-rGO prepared without competition of Ti shows poor activity and stability, which indicate vital role of Co-N_4 and TiN for remarkable catalytic ability of Co-N_4/TiN-rGO. The reaction mechanism is also proposed based on the theoretical calculation. The strategy is indicative to design Ni (Fe, Cr, Cu)-based SACs .

Introduction

The liquid-phase catalysis (oxidation of alcohols and benzene, coupling reactions, and reduction of nitroarenes etc.) plays a vital role for producing fine chemical products.[1-3] Typically, the reduction of nitro compounds to corresponding amines is one of the important processes in the fine and bulk chemical industry. The high-efficient and low-cost catalysts are necessary to promote reaction and increase the selectivity. Precious metals (Pt, Pd etc.) are most effective catalysts due to its special d-electron structure, but suffer from high cost and low abundance.[4,5] The fact impels intensive attentions on decreasing the usage of Pt (Pd) or replacing them by non-noble metals, which can be realized by tuning the shape, size and designing like-Pt catalysts (WN, Mo_2N, Mo_2C etc.).[6-8] Eventually, the decrease of size to single atom can change of electronic state of catalysts, thus tuning the adsorption/activation capacity of the reactants on single atom catalysts (SACs) for high-efficient catalysis.[9-13] The noble metal (Pt, Pd) SACs are promising for hydrogenation,[14] formic acid oxidation[15] etc. Especially, transition metal-based SACs (TM-SACs) have received extensive attention due to their low cost and specific characteristics benefited for the application in OER,[16] H_2O_2 synthesis[17] and CO_2 reduction.[18]

The SACs should be stabilized on supports through M-N (O, S etc.) bonds due to the high surface energy.[19-21] Its activity can be governed by the kind of metal elements and also the types of anion sites. The combination of TMs with N (P, C) can tune the metal d-band structure and change density of states near the Fermi level, thus regular the catalytic ability.[22,23] In this regard, the single-atom TMs (Fe, Co and Ni) stabilized by N sites on carbons can activate hydrogen (oxygen etc.) benefiting from the coordinatively unsaturated metal sites. Generally, the catalysts are obtained by the pyrolysis of the carbon source combined with metal ions. The use of excessive metals can result in the formation of large particles, which should be etched by acid and thus bring potential environmental pollution.[24-28] Moreover, some particles protected by carbons can not be completely etched. The particles are potential active sites, thus can affect the understanding of the activity origin.[29,30] Besides, the TM-N SACs embedded into carbon can be formed by pyrolysis of metal-organic framework (MOFs) precursor under NH_3 atmosphere, followed by acid leaching,[31,32] or be prepared by introducing easily vaporized Zn species into MOFs.[33] The strategy is effective but is effected by the yield and cost of MOFs to some content.[34,35] The easy synthesis of SACs

[a] Key Laboratory of Superlight Materials and Surface Technology of Ministry of Education, College of Materials Science and Chemical Engineering, Harbin Engineering University, Harbin 150001, P. R. China. E-mail: fuhg@hlju.edu.cn, fuhg@vip.sina.com;

[b] Key Laboratory of Functional Inorganic Material Chemistry, Ministry of Education of the People's Republic of China, Heilongjiang University. Harbin 150080, China chunquitianhq@163.com, tianchunqui@hlju.edu.cn.

[c] Shanghai Synchrotron Radiation Facility (SSRF), Shanghai Institute of Applied Physics, Chinese Academy of Sciences, Shanghai 201204, China;

Electronic Supplementary Information (ESI) available: [details of any supplementary information available should be included here]. See DOI: 10.1039/x0xx00000x

with good activity and stability is desirable for the practical application.

Based on the analyses on the preparation methods of most SACs, the suitable path for the preparation of the SACs should be able to easily control the metal content and dispersion on supports during the "precursor" step and to avoid the subsequent formation of large particles. The separation and stabilization of SACs by a "physical spacer", rather than only M-N (S, O) bond, is especially desirable to hinder the aggregation of SACs under the harsh catalytic conditions. The GO with abundant functional groups, a well-known support for SACs, can combine with various metal precursors to give oxides (TiO_2 or CoO etc.).[36,37] So, it is proposed that one metal species having stronger interaction with GO predominantly occupy more groups on GO, so as to control the amount and dispersion of the weaker one on GO. Here, we showed that the high positive charge of Ti species (TBT, titanium (IV) butoxide) can predominately combine with GO compared to Co^{2+} (Fe^{3+}, Ni^{2+} etc) species. Thus, most of the groups on GO can be predominantly occupied by Ti species. Only trace Co^{2+} can combine with the groups remained at the gaps of Ti species on GO. The "competitor" and "spacer" roles of Ti species makes the formation and stabilization of Co-N_4 SACs embedded in 2D TiN/rGO sheets by the nitridation without additional acid-treatment.(Scheme 1) As a result, the Co-N_4/TiN-rGO have shown excellent activity and stability by taking the reduction of aromatic nitro compounds (ANs) into amine as a proof-of-concept. The catalyst can fast convert the various ANs with high-concentration (up to 2 mM) at low temperature. The conversion rate of 4-NP to 4-AP on Co-N_4/TiN-rGO (0.098 s^{-1}) is much higher than on Co_4N/rGO (0.037 s^{-1}) which is prepared without "competitive occupancy" of Ti species. The catalyst have shown superior stability with no loss of activity after 15 times of reuses. The activity and stability is at the forefront of the reported catalysts. The strategy is also indicative to design Ni (Fe, Cr, Cu)-based SACs by the competitive occupancy of corresponding metal salts with TBT.

Experimental Section

Materials and chemicals

Cobalt nitrate ($Co(NO_3)_2•6H_2O$), iron nitrate($Fe(NO_3)_3•9H_2O$), nickel nitrate ($Ni(NO_3)_2•6H_2O$), chromium nitrate ($Cr(NO_3)_3•9H_2O$), cupric nitrate ($Cu(NO_3)_2•3H_2O$), titanium (IV) butoxide ($Ti(OBu)_4$), cyclohexane and ethanol (C_2H_6O, 99.0%) were purchased from Aladdin Co., China. P-nitrophenol ($C_6H_5NO_3$) and Sodium borohydride ($NaBH_4$) was purchased from Sinopharm Chemical Reagent Co., Ltd. All chemical reagents were used as received without further purification. Distilled water was obtained from an analytical laboratory.

Preparation of graphene oxide (GO)

Graphene oxide (GO) was synthesized from natural graphite powder by a modified Hummers method. In detail, 2 g of expanded graphite was added into 50 mL of 98 wt% H_2SO_4 in a 250 mL beaker under magnetic stirring. Then, 2 g of sodium nitrate and 6 g of $KMnO_4$ was added slowly to the dispersion in sequence, which was remained at 28°C water bath for 20 h under magnetic stirring. Finally, 80 mL of distilled water and 20 mL of 30% H_2O_2 aqueous solution were added into the reaction system, followed by washing with 2 mM HNO_3 aqueous solution. Graphene oxides were obtained after centrifuging (12000 rpm), washing with alcohol and drying.

The preparation of M-N/TiN-rGO

0.1 g of graphene oxide (GO) were dispersed into 10 mL of alcohol followed by a sonication for 1 h. Then, 30 mL of cyclohexane was added to the dispersion. A certain amount of Cobalt nitrate and TBT was dropwised into GO dispersion and stirred for 12 h at room temperature. After that, the dispersion was centrifuged and washed three times with cyclohexane to remove the remained TBT and cobalt nitrate in solvent. Next, the solids were re-dispersed into 45 mL cyclohexane and then transferred to a 100 mL autoclave and kept in an electric oven at 180°C for 5 h. The product was collected after centrifugation, then washed with ethanol for several times, and dried in oven at 40°C. Finally, the solids were calcinated at NH_3 atmosphere with a heating rate of 3°C min^{-1} to 800°C and maintained at this temperature for 2 h (flow rate is 40 sccm). As obtained black solids were named as Co-N_4/TiN-rGO. In order to study the influence of TBT on the "competitive occupancy" process, the amounts of TBT were tuned from 0 mL to 6 mL. The samples obtained in the absence of Ti species was named as Co_4N-rGO. The samples and corresponding preparation conditions were listed in Table S1. The procedures for the synthesis of Fe-N/TiN-rGO, Ni-N/TiN-rGO, Cr-N/TiN-rGO and Cu-N/TiN-rGO nanostructures were similar to that of Co-N/TiN-rGO excepting the use of the corresponding metal salts instead of cobalt salt.

Characterizations

Wide-angle X-ray diffraction (XRD) was recorded in the 2θ range of 10-80° on a Bruker D8 Advance X-ray diffractometer with CuKα (λ = 1.5418 Å) radiation (40 kV, 40 mA). Thermogravimetric (TG) analysis was obtained on a SDT Q600 instrument with a constant flow of air. The scanning electron microscopy (SEM) mappings were obtained on a scanning electron microscope (Hitachi S-4800) with an acceleration voltage of 5 kV. The transmission electron microscopy (TEM) and high-resolution TEM (HRTEM) tests were performed using a JEM-F200 electron microscope (JEOL, Japan) with an acceleration voltage of 200 kV. Carbon-coated copper grids were used as sample holders. X-ray photoelectron spectroscopy (XPS) analysis was carried out on a VG ESCALABMK II with a Mg Kα achromatic X-ray source. The content of Co and Ti was determined with a inductively coupled plasma-optical emission spectrometry (ICP-OES, PerkinElmer Optima 7000DV analyzer). Ultraviolet-visible (UV-vis) spectra were recorded using a spectrophotometer (UV-1800B). Raman spectra was collected by using a Jobin Yvon HR 800 micro-Raman spectrometer with a 457.9 nm laser as excitation source. The XAFS at Co K-edge was recorded at a transmission mode by using ion chambers at beam line BL14W1 of the Shanghai Synchrotron Radiation Facility (SSRF) of China with a Si (111) double-crystal

monochromator. The photon energy was calibrated with Co standard foil.

The Catalytic Reduction of 4-Nitrophenol by $NaBH_4$ on different catalyst.

In a typical procedure, 5.0 mg of catalyst was dispersed into 2 mL distilled water via sonication. 3 mL (3 mM) of a 4-NP aqueous solution was mixed with 25 mL of distilled water in a weighing bottle (40 mm × 70 mm). The bottle was immersed in a thermostatic water bath and then $NaBH_4$ (8 mg) was added into the dispersion. The concentration of 4-NP after dilution is 0.3 mM. The conversion of 4-NP to 4-AP was initiated by adding catalyst (5 mg) to the deep-yellow dispersion. The reaction progress was timely monitored by UV-vis spectrophotometer. In reused test, the catalyst was separated via centrifugation and washing with doubly distilled water. After drying at 60°C, the catalyst was re-used for the next cycling reaction. The catalytic activity of Co-N_4/TiN-rGO was tested at different temperatures (5-45°C) according to above procedure. In addition, the catalytic activity of Co-N_4/TiN-rGO was evaluated by using higher concentrations of p-nitrophenol (1-2 mM). For comparison, the control experiments were also carried out under similar conditions by using rGO, TiN/rGO and Co_4N-rGO as the catalyst at 25°C. Furthermore, the catalytic reduction of other nitroarenes were also performed followed the same procedures at 25°C.

Theoretical calculation

The theoretical calculations are performed within the framework of density functional theory (DFT) embedded in CASTEP code. The exchange-correlation energy is treated with generalized gradient approximation (GGA), using the Perdew-Wang parametrization. The electronic wave functions at each k-point are expanded in terms of a plane-wave basis set, and an energy cutoff of 380 eV is employed. The ultrasoft pseudopotential (USP) is used, which allows the calculations to be performed with the lowest possible energy cutoff for the plane-wave basis set. The whole optimization procedure is repeated until the average force on the atoms is less than 0.01 eV/Å and the energy change less than 5.0×10^{-6} eV/atom. The sampling over the Brillouin zone is treated by a (2×2×2) Monkhorst-Pack mesh. The thickness of vacuum was 15 Å to make sure that there was no superficial interaction between different layers.

Results and discussion

Material preparation and characterizations

We have proposed a “competitive occupancy” strategy toward the conventional synthesis and stabilization of SACs. In the route, the metal species (M_1) having stronger interaction with GO can act the "competitor” and “spacer” of weaker one (M_2). We have demonstrated the idea by taking the Ti species (TBT, titanium (IV) butoxide, M_1) and Co species (Co^{2+}, M_2) as a proof-of-concept. The $Co(NO_3)_2$ and TBT are combined with GO by competitive occupancy. The role of TBT as "competitor” can be directly reflected by the colors of the supernatant after the adsorption of Co precursor (10 mg) on GO in the presence of different amount of TBT (0-6 mL) (Figure S1). Without adding TBT, the supernatant have no distinct color, indicating the complete combination of Co^{2+} with GO. The addition of 1.5 mL TBT can make a pale pink color of the supernatant, implying the little combination of Co^{2+} with GO. The presence of 3 mL (or 6 mL) of TBT leads to deeper color of supernatant close to the original ones, indicating the combination of trace Co^{2+} with GO. The TG analyses (Figure S2 and Table S2) show that the amount of Ti on the final Co-N/TiN-rGO increased from 12.8% to 26.6% and 27.1% as the addition of 1.5 mL, 3 mL and 6 mL of TBT. Obviously, the amount of Ti species on GO increases with the increase of TBT amount. The adsorption amount is close to saturation as the addition of 3 mL of TBT. The inductively coupled plasma optical emission spectrometry (ICP-OES) analysis have revealed 0.428 wt%, 0.136 wt% and 0.08 wt% Co amount, corresponding to the use of 1.5 mL, 3 mL and 6 mL TBT during the “competitive occupancy” process. The “competitive occupancy” is also existence between the TBT and other metal ions (Ni, Fe and Cr etc.).

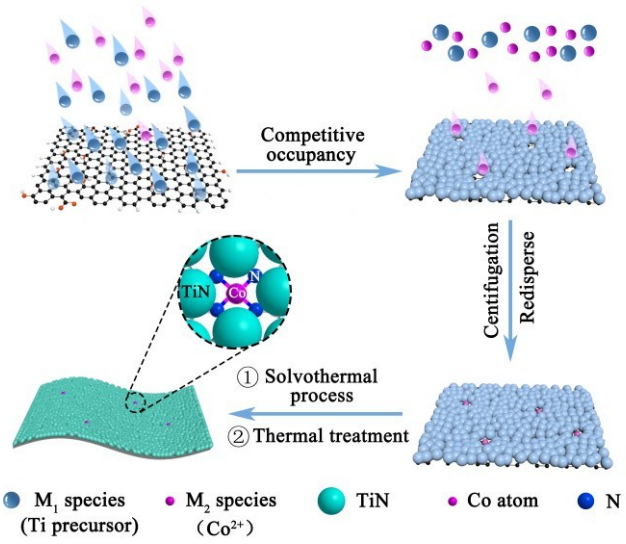

Scheme 1. Schematic process of “competitive occupancy” for the synthesis of Co-N_4/TiN-rGO.

Above results show that the amount of Co species on GO can be controlled by “competitive occupancy” of Ti species. An appropriate amount of Co can combine with GO by using 3 mL TBT. So, the sample prepared in the case (named Co-N_4/TiN-rGO, ESI) was characterized in detail to verify the effectiveness of present strategy toward stable Co-N SACs. The precursor from hydrothermal treatment shown a thin two-dimensional layer structure (Figure S3). The XRD patterns of Co-N_4/TiN-rGO sample (Figure 1a) show a peak at around 26°, indexing to (002) reflection of the hexagonal graphite. The peaks located at 36°, 43°, 62° are indexed to TiN (111), (200), (220) diffractions (PDF#38-1420), respectively. No diffraction peaks of cobalt

View Article Online
DOI: 10.1039/C9TA13615K

Journal Name

ARTICLE

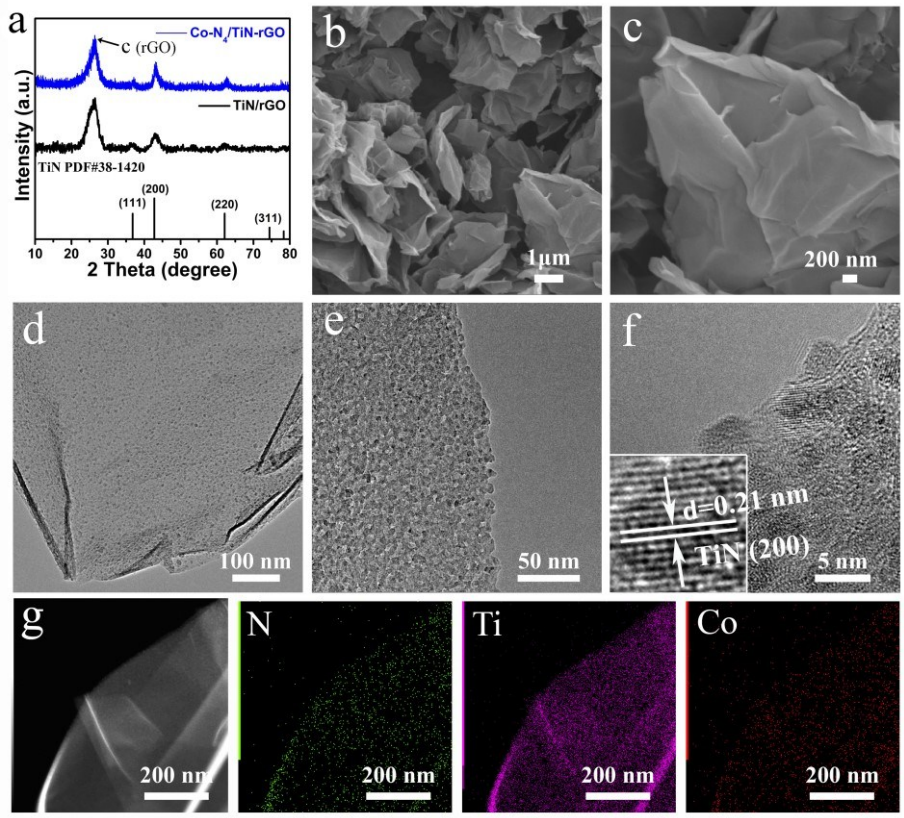

Figure 1. (a) XRD patterns of Co-N_4/TiN-rGO and TiN/rGO. (b, c) Typical SEM images, (d, e) TEM images, (f) HRTEM images and (g) EDX elemental mapping image of Co-N_4/TiN-rGO.

species are observed, which implies the low amount of Co species. Thin sheets similar to that of GO are observed by scanning electron microscopy (SEM) (Figure 1b, c), implying the small size and uniform distribution of TiN on rGO. The TEM images indicate the presence of dense and uniform particles (~5 nm) on rGO (Figure 1d, e). The high-resolution TEM (HRTEM) (Figure 1f) image shows the lattice spacing of 0.212 nm, corresponding to (200) planes of TiN.[38] The dense and uniform distribution of Ti species on rGO imply the uniform distribution of remained groups after "competitive occupancy" of Ti species, which can result in the uniform combination of Co species with rGO. The energy dispersive spectrum (EDS) elemental mapping images show the uniform distribution of Ti, C, N, and Co elements through whole sheet (Figure 1g), which suggests the high dispersion of Co species on GO. X-ray photoelectron spectroscopy (XPS) shows the formation of TiN and N-doped rGO (Figure S4), but with no obvious sign of Co element, which should be ascribed to the low content exceeding the detection limitation of XPS. The similar Raman peaks (Figure S5) for Co-N_4/TiN-rGO and TiN/rGO indicate the little effect of Co species on the structure of TiN/rGO. The characteristics of undetectable Co by XRD, TEM and XPS are consistent with that of SACs.[39]

X-ray absorption fine structure (XAFS) are robust tool to study the structure of SACs. In the normalized X-ray absorption near-edge structure (XANES) spectrum (Figure 2a), the position of the rising edge for Co in Co-N_4/TiN-rGO is between those for Co foil and CoO, indicating that the valence of Co in Co-N_4/TiN-rGO is between CoO and Co^{2+} (Figure 2b).[40] The Fourier transformed (FT) k3-weighted extended EXAFS spectrum of Co-N_4/TiN-rGO shows one main peak at 1.34 Å that belongs to Co-N first coordination shell. No other high-shell peaks are observed (Figure 2c, 2d), suggesting the formation of atomically dispersed Co-N in Co-N_4/TiN-rGO. The wavelet-transform (WT) EXAFS

View Article Online
DOI: 10.1039/C9TA13615K

analysis is further performed because it can discriminate the backscattering atoms even when they overlap substantially in R-space by providing additional k-space.

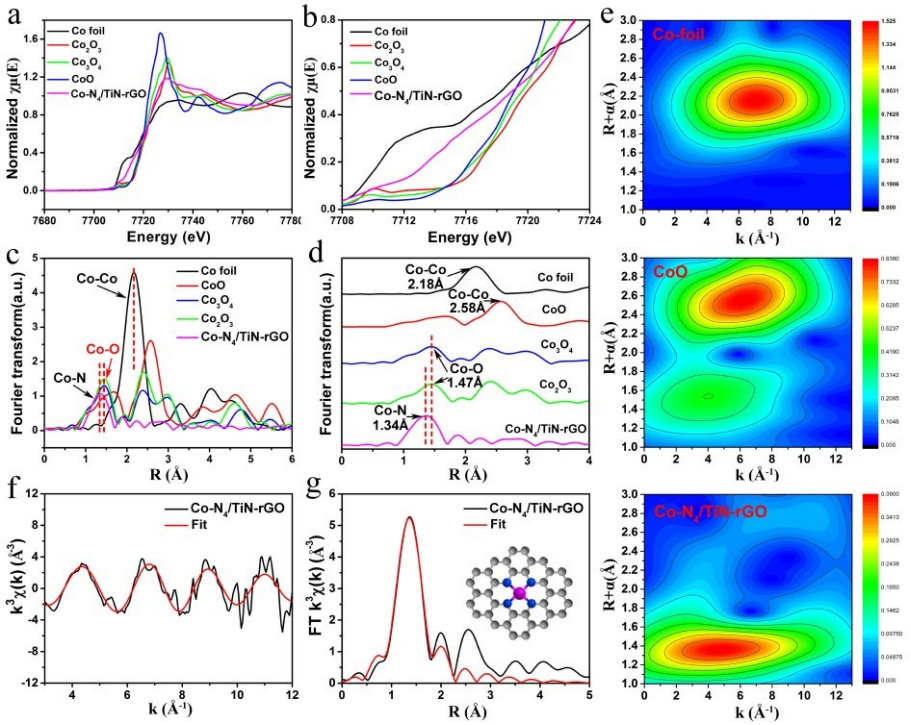

Figure 2. (a) Co K-edge XANES spectra of Co-N_4/TiN-rGO and reference samples; (b) a magnified image of Figure a; (c, d) Co K-edge k3-weighted EXAFS curves of Co-N_4/TiN-rGO and reference at Co K-edge; e) WT for the k3-weighted EXAFS signals; (f , g) the corresponding EXAFS fitting curves of Co-N_4/TiN-rGO at k and R space, inset shows the schematic model, Co (violet), N (blue) and C (gray).

The WT contour plots of Co-N_4/TiN-rGO exhibits only one intensity maximum at 4.6 Å (Figure 2e), which is assigned to Co-N coordination.[41,19] No intensity maximum corresponding to Co-Co coordination is found by comparing with that of Co foil and CoO references, which further excludes the presence of Co particles. Corresponding EXAFS fitting curves of Co-N_4/TiN-rGO at k and q space are shown in Figure 2f and 2g. Table S3 summarizes the fitting results of the EXAFS spectra of Co-N_4/TiN-rGO and Co foil. By performing EXAFS fitting, the first shell of Co atoms in Co-N_4/TiN-rGO exhibits a coordination number of 4.4 and the mean coordination situation of Co is consistent with that of Co-N_4 reported in most literature.[42,19]

There are several keys for the formation of the Co SACs on supports. First, the amount of TBT can control the amount of Co species through competitive occupancy, thus it should be tuned to give suitable loading of Co. With no "competitive occupancy" by Ti species, almost all Co species can combine with GO, leading to the formation of large Co_4N particles (Figure S7-S9). In addition, the combination of TBT on GO can be effected by solvent used in the synthesis. As shown in the Figure S10, the large block material can be formed when the distilled water was used as the solvent, which should be due to the rapid hydrolysis of the tetrabutyl titanate. In addition, the use of non-polar cyclohexane is favorable to form uniform and dense small particles on GO, while the use of ethanol can result in the formation of larger and sparse particles on GO (Figure S11). The difference should be relative with the different polarization of solvent that effect the combination of GO with Ti and Co species.

Catalytic hydrogenation performance

The aromatic nitro compounds (such as p-nitrophenol, p-NP) is a refractory organic pollutant with potential threat to human and aquatic organisms. Thus, the conversion of p-NP to p-aminophenol (p-AP) can both eliminate a pollutant and to realize the implementation of a waste into industrial manufacture.[43,44] Previous work shows the potential of CoN_4-based catalysts for the conversion of p-NP to p-AP. However, the catalysts show the moderate activity and poor reused ability, due to larger size and absence of effective protection.[45,46] The formation of Co-SACs separated by TiN should be favorable to develop the catalytic activity and stability. The 4-NP solution exhibits a strong absorption peak at 319 nm, which was red-shifted to 400 nm after the addition of $NaBH_4$ due to the deprotonation of 4-NP (Figure 3a). No

reaction occurred in the absence of the catalyst or presence of rGO or TiN/rGO, implying that the reduction could not happen in these cases (Figure 3b, 3c). In contrast, the addition of Co-N_4/TiN-rGO into the system can initiate the reduction immediately (Figure 3d). The intensity of absorption peak at 400 nm gradually decreased, in company with the emergency of an absorption peak at 300 nm due to the formation of p-AP.

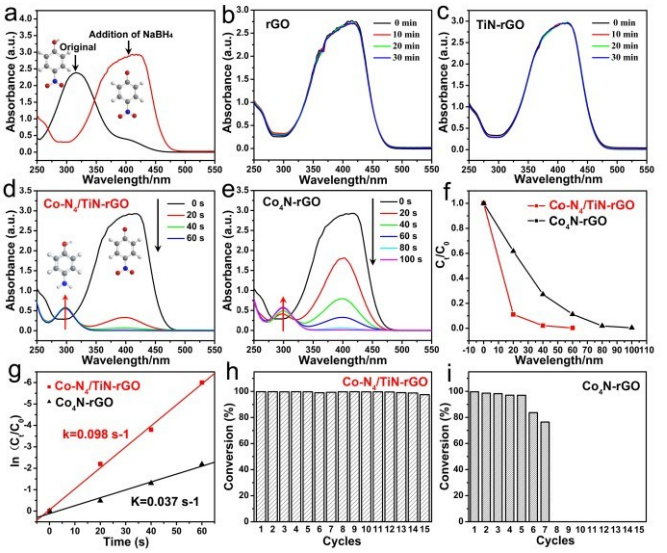

Figure 3. (a) UV absorption before and after the addition of $NaBH_4$ into 4-NP; (b, c) Absorption of the 4-NP solution at 400 nm after adding rGO and TiN/rGO in the presence of $NaBH_4$; (d, e) The change of absorption value for the solution at 400 nm in the presence of $NaBH_4$ over (d) Co-N_4/TiN-rGO, (e) Co_4N-rGO (f) C/C_0 and (g) $\ln(C/C_0)$ as a function of reaction time; (h, i) reused activity of Co-N_4/TiN-rGO and Co_4N-rGO.

The reaction proceeded rapidly with a conversion over 99% in ca. 60 s. The activity is superior to most reported catalysts.[47-50] Notably, the Co_4N-rGO show poor activity for the conversion (about 100 s, Figure 3e), indicating the promoted role of Co-N_4 SACs on the catalytic activity.

The conversion of 4-NP is calculated from C_t/C_0 by the relative intensity of UV/Vis absorbance (A_t/A_0) at 400 nm (Ct is the concentration of 4-NP at the reaction time t, and C_0 is the initial concentration). A 90% conversion is achieved in the presence of Co-N_4/TiN-rGO within 20 s of reaction, while it is less than 40% for Co_4N-rGO. The concentration of $NaBH_4$ was much higher than that of 4-NP and thus was considered as constant during the reaction. Consequently, the reduction is assumed to be pseudo-first-order with respect to the concentration of 4-NP. The rate constant (k_1) of the reaction is 0.098 s^{-1} and 0.037 s^{-1} for Co-N_4/TiN-rGO and Co_4N-rGO (Figure 3f and 3g). The conversion is still reached almost 100% of first run even after 15 cycles of Co-N_4/TiN-rGO (Figure 3h) with no obvious change in Co loading (Table S4). However, the Co_4N-rGO catalyst shows a significant decrease in the activity after 5 times of reuses (Figure 3i). To further illustrate the role of TiN, another comparative sample (Co-rGO-1) was also prepared without addition of Ti during the synthesis. The content of Co in Co-rGO-1 was same as that in Co-N_4/TiN-rGO (about 0.4%). The Co species are undetectable by XRD, SEM and TEM due to the low content of Co (Figure S12-S14). As shown in Figure S15a, much longer reaction time was required over Co-rGO-1 (180 s) for the reduction of 4-nitrophenol in comparison with that over Co-N_4/TiN-rGO (60 s) under similar conditions. The rate constant (k_1) over Co-rGO-1 was about 0.0094 s^{-1} (Figure S15b, 15c) , which is lower than that of Co-N_4/TiN-rGO (0.098 s^{-1}). Notably, the Co-rGO-1 catalyst showed a significant decrease in catalytic performance only after 4 cycles (Figure S15d). The tests indicated the advantage of the competitive occupancy process to give efficient and stable Co-N_4 based catalyst. In addition, the catalysts prepared in water and ethanol solvent have shown poor performance than those in cyclohexane (Figure S16), which is relative with the ineffective separation and stability of Co species due to the large size and poor dispersion of TiN. All the above results indicate that the TiN can act as spacer to separate Co species to form Co-N_4 during the synthesis. Besides, the Co-N_4 SACs on GO are surrounded and separated by TiN, which effectively hinders their migration and aggregation during the catalysis. Also, the hot filtration test show that the conversion cannot be happened with no assistance of Co-N_4/TiN-rGO, further indicating the excellent stability and heterogeneous characteristics of Co-N_4/TiN-rGO catalyst (Figure S17).

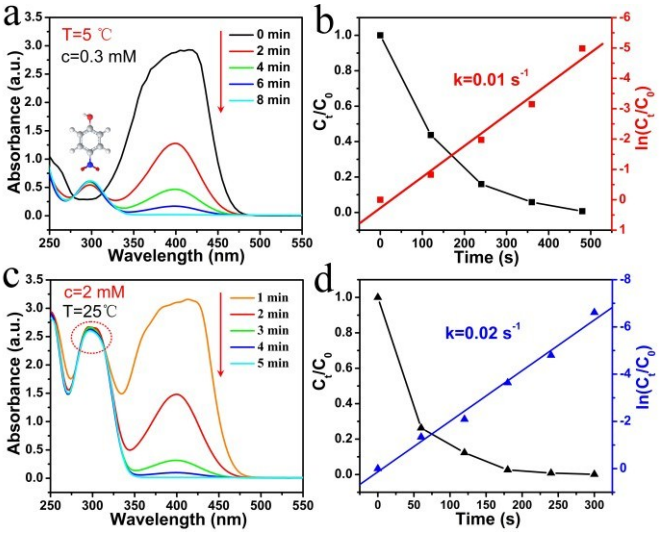

Figure 4. (a) The change of absorption value of 4-NP solution with time at 400 nm at 5°C; (b) C/C_0 and $\ln(C/C_0)$ as a function of reaction time at 5°C; (c) The change of absorption value of 4-NP solution (initial concentration of 2 mM) at 400 nm with time; (d) C/C_0 and $\ln(C/C_0)$ as a function of reaction time; The catalyst is Co-N_4/TiN-rGO.

The Co-N_4 and TiN in Co-N_4/TiN-rGO are formed by the reaction of Co and Ti species with NH_3 at certain temperature.

View Article Online
DOI: 10.1039/C9TA13615K

Therefore, the calcination temperatures also has a great influence on the catalytic performance of final materials. As shown in Figure S18, the catalyst obtained by the calcination at 800°C shows the higher catalytic activity than those from calcination at 700°C and 900°C, which indicates that too high and too low processing temperatures are not conducive to the formation of efficient Co-N_4 catalysts.

Besides good activity and stability, there are several virtues needing to be noted. First, the high activity of Co-N_4/TiN-rGO can make the fast conversion of 4-NP to 4-AP at the low ratio of $C_{NaBH4}/C_{4\text{-}NP}$ (29), while the ratio is over 100, even 1000 for many previous studies (Table S7). The use of low-amount $NaBH_4$ is more favourable for the practical use. Second, the temperature has a great influence on the catalytic performance and most of the reactions are carried out at room temperature. However, the reaction can be fast proceeded at low temperature over Co-N_4/TiN-rGO. The catalyst can still convert 4-NP to 4-AP at 1 minute and 8 minute when the reaction temperature is 15°C and 5°C, respectively (Figure 4a, 4b, Table S5). The 4-NP could be completely transformed in 45 s as increase of reaction temperature to 45°C. Third, the concentration of the 4-NP solution used in most literature is 0.1-0.3 mM. In this paper, the high concentrated 4-NP can still be effectively converted within short time. The conversion of 1 mM, 1.5 mM, and 2 mM 4-NP can reached 99% in 2 min, 3 min, and 5 min, respectively (Figure 4c, Table S6). The rate constant (k) is as high as 0.02 s^{-1} when the concentration of 4-NP is 2 mM (Figure 4e). The Co-N_4/TiN-rGO performs highest activity and stability than previously reported noble-metal and transition-metal catalysts (Tables S7). Finally, the catalyst exhibits good catalytic activity toward a series of nitroarenes compounds (Table S8). All of above are very important for the practical application. The "competitive occupancy" strategy developed here provides a feasible method for the synthesis of stable TM-SACs. Primary experiments show that the "competitive occupancy" on GO also exists between the TBT and other TM salts, such as Ni, Fe, Cr and Cu salts (Figure S19). The M-N/TiN-rGO prepared based on "competitive occupancy" strategy all show the better activity than the corresponding catalysts without the "competitive occupancy" of Ti species (Figure S20). However, the Co-N_4/TiN-rGO catalyst has very little catalytic activity for aromatic nitroreduction with H_2 and $N_2H_4{\cdot}H_2O$ as reducing agents (Figure S21 and Figure S22).

The SACs are active for thermo-, electro-, and photocatalytic reactions.[51] Some precious metal SACs have been applied to the catalytic hydrogenation of nitro compounds, but the catalytic mechanism has seldom specified. Here, we have primarily analyzed the mechanism of Co-N_4 based catalyst for catalytic reduction of nitro compounds. Density functional theory (DFT) calculations are performed to further understand the reaction process of 4-NP reduction over Co-N_4 sites. As shown above, the TiN played the role for the stabilization of Co-N_4 sites, and shown no activity for the reduction of nitro compounds. So, the calculation is performed on the Co-N_4/rGO for simplification. Figure S23 and S24 show the DFT model and intermediate products. The adsorption energy profiles along hydrogenation of 4-NP on Co-N_4/TiN-rGO are shown in Figure 5a. According to the previous reports,[52,53] we calculate the adsorption energy of the possible reaction route for reducing nitroaromatics. The hydrogenation process are monitored by simulating the adsorption energies of the intermediates. The adsorption energy of 4-NP on Co-N_4/TiN-rGO (denoted as GR-NO_2*) is about -0.48 eV, where one of the oxygen in the nitro is attached to the single Co atom.

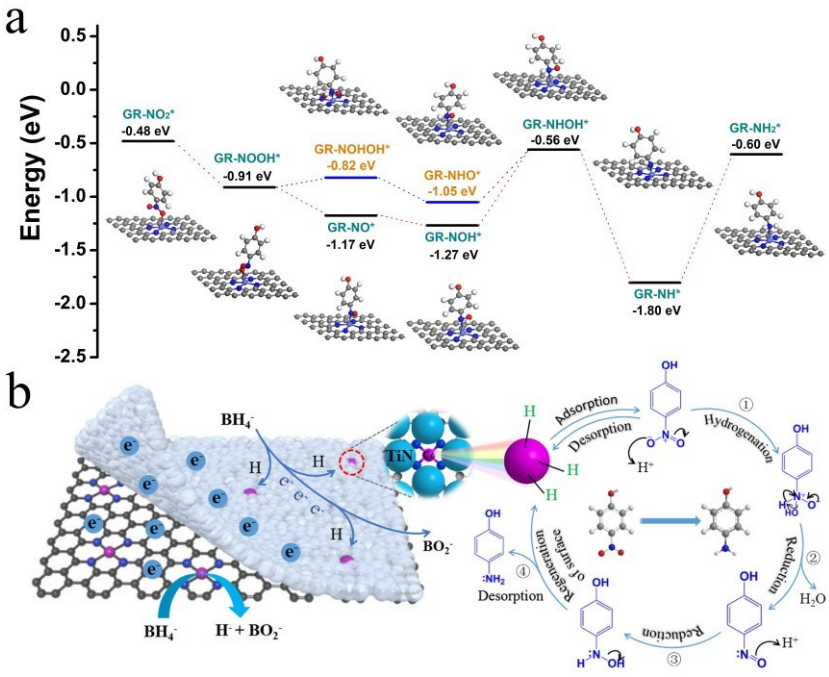

View Article Online
DOI: 10.1039/C9TA13615K

Journal Name

ARTICLE

Figure 5. (a) Stepwise hydrogenation of 4-NP on Co-N_4/TiN-rGO and the corresponding energy profiles from DFT calculations; (b) Proposed mechanism for hydrogenation of 4-NP over Co-N_4/TiN-rGO.

The first hydrogen was added to the free oxygen in the nitro and GR-NO_2* was reduced to GR-NOOH*. The adsorption energy of GR-NOOH* on Co-N_4/TiN-rGO is -0.91 eV, which is below the adsorption energy of 4-NP on Co-N_4/TiN-rGO. The result proves that the first hydrogenation process is apt to occur on the Co-N_4. For the addition of the second hydrogen, there are two different situations where the intermediates are GR-NOHOH* and GR-NO*, respectively. The results show that the GR-NO^* has lower adsorption energy and is much more stable than GR-$NOHOH^*$. Therefore, during the hydrogenation process, the GR-NO^* is predominant intermediates to GR-$NOHOH^*$. For the third hydrogenation process, the calculations show that GR-NOH^* is more stable than GR-NHO^*. The fourth hydrogen is added to the oxygen of GR-NHO^* to form GR-$NHOH^*$, and the addition of the fifth hydrogen forms GR-NH^*. The last hydrogen is attached to the nitrogen of GR-NH^* to give the final product GR-NH_2^*. Accordingly, it can be concluded that the path represented by the black line in the graph is a favourable conversion process. Based on DFT results, we have proposed the overall mechanism of 4-NP hydrogenation on Co-N_4/TiN-rGO (Figure 5b). The reduction of 4-NP by sodium borohydride is very difficult without a catalyst because high energy barrier between two negative ions. Therefore, the presence of a catalyst is very important to decrease the energy barrier, as well as for reaction being taking place on the Co-N_4. Firstly, $NaBH_4$ reacts with water to produce H and BO_2^-, and the produce H further reacts with the surface exposed Co-N to form cobalt-hydrogen (Co-H) bonds. Meanwhile, the nitroarenes are also adsorbed onto the Co site. Then, the hydrogen and electron transfer from the catalyst to the nitro group of adsorbed 4-NP, which goes through several steps of hydrogenation reactions to form the final product, 4-AP. Once amino are formed, it can desorb from the catalyst to create a free surface and the catalytic cycle starts again.

Conclusions

In summary, we have demonstrated a robust "competitive occupancy" strategy toward Co-N_4 SACs embedded in 2D TiN/rGO sheets. The Ti species can act as both "competitor" to control the amount of Co species on GO, and a "spacer" to separate the Co species, thus ensuring the easy formation and stabilization of Co-N_4 on GO. The virtues endow the high activity and stability of Co-N_4 SACs superior to reported noble metal and non-noble metals catalysts. The catalyst can convert the high-concentrated aromatic nitroarenes within short times at low ratio of $C_{NaBH4}/C_{4\text{-}NP}$ and low temperature, with no loss of activity after 15 times of reuses. Present strategy is indicative to design high-effective and stable SACs for catalytic application.

Conflicts of interest

There are no conflicts to declare.

Acknowledgements

This research is support by the National Key R&D Program of China (2018YFE0201704), the NSFC (21571054, 91961111, 21631004, 21901064, 21770159, 21805073), the Natural Science Foundation of Heilongjiang Province (YQ2019B005), the Basic Research Fund of Heilongjiang University in Heilongjiang Province (RCYJTD201801). The authors also thank the support of Shanghai Synchrotron Radiation Facility (SSRF).

Notes and references

1 D. Formenti, F. Ferretti, F. K. Scharnagl, M. Beller and *Chem. Rev.,* 2018, **119**, 2611-2680.
2 J. Pritchard, G. A. Filonenko, R. van Putten, E. J. M. Hensen and E. A. Pidko, *Chem. Soc. Rev.,* 2015, **44**, 3808-3833.
3 J. Liu, N. P. Wickramaratne, S. Z. Qiao and M. Jaroniec, *Nat. Mater.*, 2015, **14**, 763.
4 D. X. Wang, J. C. Liu, X. S. Cheng, X. Kang, A. P. Wu, C. G. Tian and H. G. Fu, *Small Methods,* 2019, **3**, 1800510.
5 T. Higaki, Y. W. Li, S. Zhao, Q. Li, S. T. Li, X. S. Du, S. Yang, J. S. Chai and R. C. Jin, *Angew. Chem.,* 2019, **131**, 8377-8388.
6 H. J. Yan, C. G. Tian, L. Sun, B. Wang, L. Wang, J. Yin, A. P. Wu and H. G. Fu, *Energy Environ. Sci*., 2014, **7**, 1939-1949.
7 A. P. Wu, Y. Xie, H. Ma, C. G. Tian, Y. Gu, H. J. Yan, X. M. Zhang, G. Y. Yang and H. G. Fu, *Nano Energy,* 2018, **44**, 353-363.
8 H. J. Yan, Y. Xie, Y. Q. Jiao, A. P. Wu, C. G. Tian, X.M. Zhang, L. Wang and H. G. Fu, *Adv. Mater.,* 2018, **30**, 1704156.
9 L. L. Zhang, M. X. Zhou, A. Q. Wang and T Zhang, *Chem. Rev.* DOI: 10.1021/acs.chemrev.9b00230.
10 J. W Su, R. X. Ge, Y. Dong, F. Hao and L. Chen, *J. Mater. Chem. A*, 2018, **6**, 14025-14042.

11 H. L. Fei, J. C. Dong, Y. X. Feng, C. S. Allen, C. Z. Wan, B. Volosskiy, M. F. Li, Z. P. Zhao, Y. L. Wang, H. T. Sun, P. F. An, W. X. Chen, Z. Y. Guo, C. I. Lee, D. L. Chen, I. Shakir, M. J. Liu, T. D. Hu, Y. D. Li, A. I. Kirkland, X. F. Duan and Y. Huang, *Nat. Catal.,* 2018, **1**, 63.
12 B. Jiang, H. Song, Y. Q. Kang, S. Y. Wang, Q. Wang, X. Zhou, K. Kani, Y. N. Guo, J. H. Ye, H. X. Li, Y. Sakka, J. Henzie and Y. Yusuke, *Chem. Sci.*, 2020, **11**, 791-796.
13 J. Liu, H. Zhang, M. Qiu, Z. H. Peng, K. H. Leung, W. F. Lin and J. Xuan, *J. Mater. Chem. A*, 2020, **DOI: https://doi.org/10.1039/C9TA11852G**.
14 Y. J. Chen, S. f. Ji, W. m. Sun, W. X. Chen, J. C. Dong, J. F. Wen, J. Zhang, Z. Li, L. R. Zheng, C. Chen, Q. Peng, D. S. Wang and Y. D. Li, *J. Am. Chem. Soc.,* 2018, **140**, 7407-7410.
15 J. Kim, C. W. Roh, S. K. Sahoo, S. Yang, J. Bae, J. W. Han and H. Lee, *Adv. Energy Mater.,* 2018, **8**, 1701476.
16 N. L. W. Septiani, Y. V. Kaneti, K. B. Fathoni, Y. Guo, Y. Ide, B. Yuliarto, X. C. Jiang, Nugraha, H. K. Dipojono, D. Golberg and Y. Yamauchi, *J Mater.Chem. A,* 2020, **DOI:10.1039/C9TA13442E.**
17 B. Q. Li, C. X. Zhao, J. N. Liu and Q. Zhang, *Adv. Mater.,* 2019, 1808173.
18 X. G. Li, W. T. Bi, M. L. Chen, Y. X. Sun, H. X. Ju, W. S. Yan, J. F. Zhu, X. J. Wu, W. S. Chu, C. Z. Wu and Y. Xie, *J. Am. Chem. Soc.,* 2017, **139**, 14889-14892.
19 Y. Q. Zhu, W. M. Sun, W. X. Chen, T. Cao, Y. Xiong, J. Luo, J. C. Dong, L. R. Zheng, J. Zhang, X. L. Wang, C. Chen, Q. Peng, D. S. Wang and Y. D. Li, *Adv. Funct. Mater.,* 2018, 1802167.
20 H. Z. Zhang, L. Shang, Q. H. Zhang, R. Shi, G. I. N. Waterhouse, L. Gu and T. R. Zhang, *Nat. Commun.,* 2019, **10**, 1-9.
21 H. H. Zhang, L. Yu, T. Chen, W. Zhou and X. W. Lou, *Adv. Funct. Mater.,* 2018, **28**, 1807086.
22 Z. W. Chen, L. X. Chen, C. C. Yang and Q. Jiang, *J. Mater. Chem. A*, 2019, **7**, 3492-3515.
23 C. F. Chen, A. P. Wu, H. J. Yan, Y. L. Xiao, C. G. Tian and H. G. Fu, *Chem. Sci.,* 2018, **9**, 4746-4755.
24 L. L. Fan, P. F L, X. C. Yan, L. Gu, Z. Z. Yang, H. G. Yang, Sh. L. Qiu and X. D. Yao, *Nature commun.,* 2016, **7**, 10667.
25 R. Zhang, L. Jiao, W. J. Yang, G. Wan and H. L. Jiang, *J. Mater. Chem. A,* 2018**, 6**, 8793-8814.
26 M. D. Hossain, Z. Liu, M. Zhuang, X. G. Yan, L. Xu, C. A. Gadre, A. Guda, A. Tyagi, I. H. Abidi, C. J. Sun, H. Wong, A. Guda, Y. F. Hao, X. Q. Pan, K. Amine and Z. T. Luo, *Adv. Energy Mater*., 2019, **9**, 1803689.
27 Y. Hou, M. Qiu, M. G. Kim, P. Liu, G. Nam, T. Zhang, X. D. Zhuang, B. Yang, J. Cho, M. W. Chen, C. Yuan, L. C. Lei and X. L. Feng, *Nat. Commun.,* 2019, **10**, 1392.
28 H. P. Yang, Y. Wu, G. D. Li, Q. Lin, Q. Hu, Q. L. Zhang and J. H. Liu, *J. Am. Chem. Soc.,* 2019, DOI: 10.1021/jacs.9b04907.
29 H. Yan, C. L. Su, J. He and W. Chen, *J. Mater. Chem. A,* 2018**, 6**, 8793-8814.
30 L. Tang, X. G. Meng, D. H. Deng and X. H. Bao, *Adv. Mater.,* 2019, 1901996.
31 L. J. Li, J. X. He, Y. Wang, X. X. Lv, X. Gu, P. C. Dai, D. D. Liu and X. B. Zhao, *J. Mater. Chem. A,* 2019, **7**, 1964-1988.
32 E. G. Luo, H. Zhang, X. Wang, L. Q. Gao, L. Y. Gong, T. Zhao, Z. Jin, J. J. Ge, Z. Jiang, C. P. Liu and W. Xing, *Angew. Chem. Int. Ed.,* 2019, **58**, 12469-12475.
33 Q. Yang, C. C. Yang, C. H. Lin and H. L. Jiang, *Angew. Chem. Int. Ed.,* 2019, **58**, 3511-3515.
34 X. C. Yang, J. K. Sun, M. Kitta, H. Pang and Q. Xu, *Nat. Catal.,* 2018. **1**, 214.
35 J. F. Zhang, C. B. Liu and B. Zhang, *Small Methods*, 2019, 1800481.
View Article Online
DOI: 10.1039/C9TA13615K
36 A. A. AbdelHamid, Y. Yu, J. H. Yang and J. Y. Ying, *Adv. Mater*., 2017, **29**, 1701427.
37 B. J. Jiang, C. G. Tian, Q. j. Pan, Z. Jiang, J. Q. Wang, W. S. Yan, H. G. Fu, *J. Phys. Chem. C*, 2011, **115**, 23718-23725.
38 T. H. Zhou, W. Lv, J. Li, G. M. Zhou, Y. Zhao, S. X. Fan, B. L. Liu, B. H. Li, F. Y. Kang and Q. H. Yang, *Energy Environ. Sci.,* 2017, **10**, 1694-1703.
39 L. M. Wang, W. L. Chen, D. D, Zhang, Y, P. Du, R. Amal, S. Z. Qiao, J. B. Wu and Z. Y. Yin, *Chem. Soc. Rev.,* 2019, DOI: 10.1039/c9cs00163h.
40 X. Liu, L. Wang, P. Yu, C. G. Tian, F. F. Sun, J. Y. Ma, W. Li and H. G. Fu, *Angew. Chem.,* 2018, **130**, 16398-16402.
41 P. Yu, L. Wang, F. F. Sun, Y. Xie, X. Liu, J. Y. Ma, X. W. Wang, C. G. Tian, J. H. Li and H. G. Fu, *Adv. Mater.,* 2019, 1901666.
42 Y. H. Han, Y. G. Wang, W. X. Chen, R. R. Xu, L. R. Zheng, J. Zhang, J. Luo, R. A. Shen, Y. Q. Zhu, W. C. Cheong, C. Chen, Q.Peng, D. S. Wang, Y. D. Li, *J. Am. Chem. Soc.*, 2017, **139**, 17269-17272.
43 L. Shang, Y. H. Liang, M. Z. Li, , G. I. N. Waterhouse, P. Tang, , D. Ma, L. Z. Wu, C. H. Tung and T. R. Zhang, *Adv. Funct. Mater.*, 2017, **27**, 1606215.
44 J. Q. Li, L. X. Zhong, L. M. Tong, Y. Yu, Q. Liu, S. C. Zhang, C. Yin, L. Qiao, S. Z. Li, R. Si and J. Zhang, *Adv. Funct. Mater.,* 2019, **29**, 1905423.
45 D. Formenti, F. Ferretti, F. K. Scharnagl and M. Beller, *Chem. Rev.,* 2018, **119**, 2611-2680.
46 L. Zhang, A. P. Wu, M. Tian, Y. L. Xiao, X. Shi, H. J. Yan, C. G. Tian and H. G. Fu, *Chem. Commun.,* 2018, *54*, 11088-11091.
47 B. Li, J. G. Ma and P. Cheng, *Angew. Chem. Int. Ed.,* 2018, **57**, 6834-6837.
48 S. Choi and M, Oh, *Angew. Chem. Int. Ed.,* 2019, **58**, 866-871.
49 Y. K. Long, Y. X. Huang, X. W. Shi and L. Xiao, *J Mater.Chem. A*, 2018, **6**, 18561-18570.
50 R. Yan, Y. Zhao, H. Yang, X. J. Kang, C. Wang, L. L. Wen and Z. D. Lu, *Adv. Funct. Mater.,* 2018, **28**, 1802021.
51 S. Mitchell, E. Vorobyeva and J. Pérez-Ramírez, *Angew. Chem. Int. Ed.,* 2018, **57**, 15316-15329.
52 J. Q. Li, L. X. Zhong, L. M. Tong, Y. Yu, Q. Liu, S. C. Zhang, C. Yin, L. Qiao, S. Z. Li, R. Si and J. Zhang, *Adv. Funct. Mater.*, 2019, **29**, 1905423.
53 L. J. Lei, Z. W. Wu, H. Liu, Z. F. Qin, C. M. Chen, L. Luo, G. F. Wang, W. B. Fan and J. G. Wang, *J Mater. Chem. A*, 2018, **6**, 9948-9961.

View Article Online
DOI: 10.1039/C9TA13615K

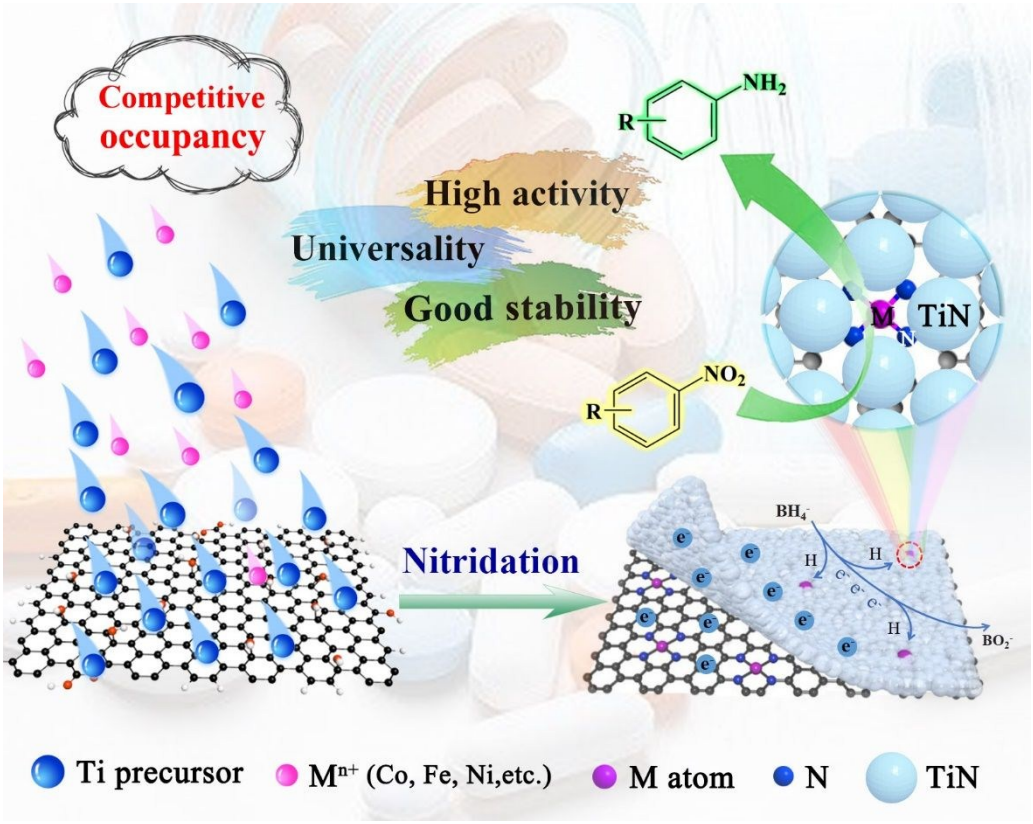

The single-atom M-N_4 based catalysts have been synthesized based on the "competitive occupancy" of Ti and Co^{2+} (Ni^{2+}, Fe^{3+}, Cr^{3+}, Cu^{2+}) on GO, in which the Ti species act as "competitor" to control the amount and dispersion of M^{n+} species, and as "spacer" to separate and stabilize M-N_4. The M-N_4/TiN-rGO can be used as high active and stable hydrogenation catalysts.